nature

https://doi.org/10.1038/s41586-026-10263-7

Accelerated Article Preview

Markovnikov hydroamination of terminal alkenes via phosphine redox catalysis

Received: 25 August 2025

Accepted: 11 February 2026

Accelerated Article Preview
Published online: 23 February 2026

Cite this article as: Fan, F. et al. Markovnikov hydroamination of terminal alkenes via phosphine redox catalysis. *Nature* https://doi.org/10.1038/s41586-026-10263-7 (2026)

Flora Fan, Kassandra F. Sedillo, Alexander J. Maertens & Abigail G. Doyle

Markovnikov hydroamination of terminal alkenes via phosphine redox catalysis

Authors: Flora Fan[1], Kassandra F. Sedillo[2], Alexander J. Maertens[1], Abigail G. Doyle[1]*

Affiliations:

[1]Department of Chemistry & Biochemistry, University of California, Los Angeles; California 90095, United States.

[2]Department of Chemistry, Princeton University; Princeton, New Jersey 08540, United States.

*Corresponding author. Email: abigaildoyle@g.ucla.edu

Summary: Main-group catalysts that mimic transition metal reactivity can expand substrate tolerance and enable transformations not currently possible with metal catalysis[1] . The discovery that P^{III} and P^{V} phosphorus intermediates can undergo transition metal-like two-electron chemistry raises the question whether radical P^{IV} intermediates can mimic other elementary steps in organometallic chemistry[2,3] . Here we describe a phosphine-photoredox catalyst system that promotes intermolecular Markovnikov hydroamination of unactivated terminal alkenes with numerous classes of N–H azoles, a reaction that is not possible with late transition metal catalysis. Experimental and computational mechanistic studies support a new elementary step for main group catalysis wherein a phosphine radical cation activates the alkene to nucleophilic amination by the azole, a step otherwise associated with transition metals. Given the broad value of nucleophilic alkene functionalization in transition metal catalysis, this P^{IV} mechanism could offer new opportunities for main group element catalysis and chemical synthesis.

Main text

Catalytic methods to construct carbon-nitrogen (C–N) bonds are widely sought due to the prevalence of amine functionality in molecules within the biomedical, agrochemical, and fine chemical industries. Hydroamination, the formal addition of an N−H bond across an unsaturated C−C bond, is a particularly valuable transformation for C(sp^3)–N bond formation because it exploits the abundance and structural variety of alkene and amine starting materials to form products with high atom economy under redox neutral conditions[4,5] . However, these reactions do not occur without a catalyst. Late transition metal (TM) catalyzed-alkene hydroamination has been extensively developed[6–8], taking advantage of different elementary steps involving a metal and alkene, such as (i) migratory insertion, (ii) nucleophilic attack on a metal-alkene complex, or (iii) metal-catalyzed hydrogen atom transfer (MHAT) (Fig. 1A)[9,10]. Despite the numerous catalysts identified and synthetic advances resulting from their development, a general solution to catalytic intermolecular, Markovnikov hydroamination of unactivated, terminal alkenes is not available[8], and only limited examples exist for this reaction class using azoles as nitrogen sources[11–13]. Since unactivated terminal alkenes are produced on manufacturing scale and comprise a significant portion of the feedstock[14,15], and azoles are widely represented in medicinal chemistry, materials science, and agrochemistry[16], they both offer underutilized and attractive substrate classes for C(sp^3)–N bond formation via hydroamination.

In 2014, the Hartwig group reported that an Ir catalyst promotes addition of indoles to terminal aliphatic alkenes via turnover-limiting migratory insertion to give hydroamination products with Markovnikov selectivity[11]. More recently, the Akai and Zhang groups described an MHAT approach to Markovnikov-selective hydroaminations between terminal aliphatic alkenes and benzotriazoles using Co catalysis, where only singular examples of other azoles, tetrazole and

benzimidazole, were demonstrated[12,13]. The specificity of these solutions to a singular azole class can be attributed to the propensity of transition metals to undergo deactivation by azole coordination[17,18] or unproductive side reactions, such as azole oxidative addition[19,20]. More generally, progress in this area has been impeded by the fact that unactivated, terminal alkenes are weak ligands for transition metals and side products arising from alkene isomerization commonly outcompete the desired, often thermally neutral, transformation[6–8,21].

Recently, researchers have sought to mimic elementary steps of transition metals using abundant main-group elements and develop main-group catalysts that expand reactivity in synthetic reactions that are challenging for transition metal catalysis[1,2,22,23]. Organophosphorus derivatives have been shown to undergo two-electron reduction/oxidation, oxidative addition, ligand exchange, and reductive elimination in stoichiometric contexts[24–26], and have emerged as versatile redox active main-group catalysts for C–F and C–N bond formation (Fig. 1B)[27–30]. In addition to representing sustainable alternatives to late transition metals, organophosphorous derivatives often show complementary functional group compatibility, such as to Lewis basic substrates. With this in mind, we questioned whether it might be possible to mimic the elementary steps involved in TM-catalyzed nucleophilic alkene functionalization with a phosphine catalyst, and in so doing, develop a generally applicable catalytic method for intermolecular, Markovnikov-selective hydroamination of azoles and unactivated terminal alkenes (Fig. 1C).

Here, we report a cooperative phosphine-photoredox catalyst system that achieves Markovnikov hydroamination between a broad range of N–H azoles and terminal, aliphatic alkenes (Fig. 1D). Our experimental and computational mechanistic studies indicate that phosphine radical cations promote nucleophilic amino-phosphination of alkenes via two competing, energetically feasible pathways, (ia/ib) and (ii) in Fig. 1C, which mimic inner- and

outer-sphere mechanisms for TM-catalyzed alkene functionalization in industrially important reactions, such as the Pd-catalyzed Wacker process and Pd-catalyzed alkene amination[31,32]. However, because the phosphine-catalyzed mechanism is initiated by an open-shell P^{IV} species, polar addition of the nucleophile is accompanied by either a radical migratory insertion or an intramolecular electron transfer into the adjacent P–C anti-bonding orbital, the latter of which represents an unusual example of the microscopic reverse of a spin-center shift process[33]. Subsequent functionalization of the resulting M–C bond proceeds via a one-electron (M = P) rather than two-electron (M = TM) mechanism, which is also distinct from most TM-catalyzed nucleophilic alkene functionalization reactions. We anticipate that these similarities and differences will offer new opportunities for the design of synthetic transformations using phosphine catalysis.

Reaction Development

Previously, our laboratory reported that PCy_3 catalyzes the hydroamination of alkenes with primary sulfonamides[34] and in collaboration with the Knowles group, hydroamination of alkenes with N–H azoles[35], both mediated by a visible light photoredox co-catalyst in a $P^{(III/IV)}$ cycle. These reactions proceeded with anti-Markovnikov selectivity, consistent with a mechanism involving the generation of a nitrogen-centered radical that undergoes anti-Markovnikov addition to the alkene. During our recent exploration of a low-performing substrate combination, the reaction of 3-phenyl pyrazole with methylene cyclopentane, we discovered that use of $P(p\text{-OMePh})_3$ as catalyst unexpectedly afforded a complete switch in regioselectivity to Markovnikov hydroamination. Since this regioselectivity outcome is prevalent for late TM-catalyzed alkene hydrofunctionalization reactions, we were intrigued by the underlying mechanism of the reaction and its synthetic implications. To this end, we sought to optimize the reaction for unactivated,

terminal alkenes, explore its synthetic scope, and understand the phosphine-dependent change of mechanism for C(sp^3)–N bond formation.

With 1-hexene as the alkene partner, we found that using 20 mol% of either P(*p*-OMePh)$_3$ or PPh$_3$, 2 mol% of [Ir(dF(Me)ppy)$_2$(dtbbpy)]PF$_6$ photocatalyst, and 10 mol% of 2,4,6-tri*iso*propylbenzenethiol (TRIP-SH) catalyst with 450 nm LEDs gave high yield and exclusive Markovnikov selectivity for the intermolecular hydroamination with 3-phenylpyrazole (**1**) to form *N*-alkylated product **2** (entries 1 and 2, extended data Table 1). Reducing the phosphine catalyst loading to 10 mol% significantly hindered activity (entry 3, extended data Table 1). Notably, other triaryl and alkylphosphine catalysts were unreactive (see supplementary materials, Table S3). Increasing the thiol loading led to reduced yield of product **2** (entries 4–6) with concomitant increase in formation of phosphonium byproduct **B1**. Given the unique regioselectivity outcome of the hydroamination, we questioned whether trace transition metal may be present. Including 10 mol% of Pd(OAc)$_2$ (entry 7) or other metal salts such as Cu(OAc)$_2$, NiBr$_2$, or Fe(OTf)$_3$ (see supplementary materials, Table S2) as an additive completely shut down reactivity. Furthermore, control studies indicated no reactivity without light (entry 11), which is inconsistent with the presence of trace amounts of a transition metal impurity serving to catalyze the reaction. While using only 1 equivalent of alkene led to reduced yield at 18 h (entry 12), the yield could be restored by allowing the reaction to run for 48 hours (entry 13), demonstrating the utility of the method for Markovnikov hydroamination of more valuable alkene coupling partners. Notably, most late TM-catalyzed hydroamination reactions with aliphatic terminal alkenes require a large excess of reaction partner (>5 equiv.) due to the weak binding of these substrates, regardless of the amine identity[8,36,37].

Azole and Alkene Scope

Next we sought to evaluate the scope of N–H azoles tolerated in the reaction (Fig. 2). We began our exploration with substituted pyrazoles, as this heterocycle class is one of the ten most common in U.S. FDA-approved drugs[16]. In addition to 3-phenylpyrazole, 3-carboethoxypyrazole (**3**) is a competent substrate, undergoing Markovnikov-selective hydroamination in 78% yield. Although a pyrazole bearing a boronic ester substituent reacted in 36% yield (**4**), the utility of boronate esters for further derivatization by cross-coupling indicates the moderate success of this substrate is nonetheless a useful advance. Fomepizole (**5**), an alcohol dehydrogenase inhibitor, was *N*-alkylated in 57% yield. 4-phenylimidazole (**6**), belonging to another highly prevalent heterocycle class in medicinal chemistry, underwent hydroamination in good yield. Biologically active compounds with the imidazole core, such as the neurotransmitter histamine (**7**) and the sedative dexmedetomidine (**8**) reacted with exclusive *N*-site selectivity.

Fused bicyclic heterocycles which contain multiple sites (at nitrogen(s) or carbon) on both rings for possible alkylation, were also amenable to hydroamination under the same set of conditions. For example, unsubstituted indazole (**9**), 3-chloroindazole (**10**), which contains a halide handle for downstream cross-coupling, and 5-fluoroindazole (**11**), which provides a medicinally relevant fluorine substituent[38], underwent hydroamination in good yield. Despite its steric hinderance, 7-methoxyindazole afforded 50% yield of product **12** under the standard reaction conditions. In the PCy_3-catalyzed anti-Markovnikov selective hydroamination[35], 4-azabenzimidazole favored the *N*3-alkylated isomer using methylene cyclopentane as an alkene partner (*N1:N3 r.r.* 1:1.2). By comparison, 4-azabenzimidazole results in exclusively the *N*1-alkylated isomer **14** under these Markovnikov-selective conditions using P(*p*-OMePh)$_3$ as catalyst, pointing to a distinct mechanism for C–N bond formation.

Incorporating another nitrogen atom in the form of 1,2,4-triazole (**15**) did not impact *N*-site selectivity, and the reaction proceeded with exclusive *N*1-alkylation. The indole core (**16**) is abundant in bioactive compounds, and 4-, 5-, 6-, and 7-azaindoles (**17–20**) were all competent substrates under the catalytic conditions, providing a useful handle to perform nitrogen scanning in medicinal chemistry library campaigns[39]. Interestingly, carbazole (**21**), oxindole (**22**), a partially saturated N–H azole, thio- (**23**) and benzo- (**24**) ureas, and fully saturated carbamate (**25**), were also reactive in this hydroamination method, demonstrating that nitrogen nucleophiles other than unsaturated azoles are compatible. While the standard reaction conditions call for the use of a glovebox, setting up the reaction under ambient conditions followed by N_2 sparging or using standard Schlenk technique demonstrated similar reactivity; products **2** and **6** were obtained in 76 and 68% yield with N_2 sparging and Schlenk technique versus 85 and 75% yield using the glovebox, respectively. Furthermore, the model reaction with 3-phenylpyrazole proved scalable in batch to gram-scale (see section 5 in supplementary materials for further details), demonstrating the potential utility of this photocatalytic protocol for industrial applications. An additive screen showcased aryl chlorides, bromides and triflates to be compatible under the reaction conditions, demonstrating complementary functional group tolerance to TM-catalyzed methods. Additives containing functional handles susceptible to oxidation or reduction under photochemical conditions (e.g. aniline, phenol etc.) were unsurprisingly less tolerated in the reaction.

Next, we surveyed the scope of terminal alkenes (Fig. 2). Unactivated monosubstituted terminal aliphatic alkenes such as 1-decene (**26**) proceeded with good yield, and various polar functional groups, including acetals (**27**), ester (**28**), and Boc-protected amines (**29**) were well-tolerated, providing additional handles for downstream derivatization of the products. Lewis-basic heterocycles, such as a pyridine moiety (**30**), did not impact reactivity. Allylbenzene, a substrate

that is susceptible to alkene isomerization with transition metal catalysts[40], led to a single *N*-alkylation product (**31**) under the phosphine-catalyzed reaction conditions. Furthermore, the structurally similar estragole, a naturally abundant phenylpropene, afforded the hydroaminated product (**32**) in 69% yield.

Additionally, terminal alkenes bearing di-substitution at the allylic position, such as vinylcyclohexane (**33**), proceeded with high yield under these phosphine/photoredox conditions. 3,3-Dimethyl-1-butene (**34**), which may undergo a 1,2-methyl shift to a more stable carbocation once coordinated to a transition metal center, underwent hydroamination in excellent yield. Whereas alcohols could serve as competing nucleophiles, the tertiary alcohol was also compatible, likely due to its steric encumbrance, and afforded a privileged 1,2-aminoalcohol scaffold (**35**). Bioactive alkenes derived from natural products and steroids, such as *(L)*-borneol (**36**) and cholesterol (**37**), gave a 1:1 mixture of diastereomeric *N*-alkylated products in high yield, and hydroamination was selective for the terminal rather than internal alkene. Despite the inclusion of a nucleophilic phosphine catalyst, the insect repellant nootkatone (**38**) could also be employed chemoselectively for reaction with the terminal alkene, bypassing potential competitive Baylis–Hillman reactivity with the enone and delivering a highly congested C–N bond. The low yield likely results from 1,1-disubstitution of the starting alkene, as also illustrated by (**39**), suggesting the steric profile of the alkene to be a significant factor in reactivity. Styrene (**40**), an activated terminal alkene, underwent Markovnikov hydroamination with 3-phenylpyrazole in 65% yield. Whereas internal alkenes (**41**) and (**42**) displayed low reactivity, the hydroamination regioselectivity was strongly phosphine-dependent, with P(*p*-OMePh)$_3$ delivering greater Markovnikov or exclusively Markovnikov selectivity, respectively, compared to that obtained with PCy$_3$ in these case studies. Overall, this hydroamination method effectively couples together a

range of N–H azoles and functionalized terminal alkenes with exclusive *N*-site selectivity and Markovnikov regioselectivity, encompassing substrates both compatible and incompatible with transition-metal catalysis under a general set of conditions.

Mechanistic Investigation

Given the well-precedented use of transition metals for Markovnikov-selective nucleophilic alkene functionalization, we hypothesized that PAr_3-catalyzed Markovnikov selectivity could result from a mechanism analogous to metal catalysis, such as (i) migratory insertion, (ii) nucleophilic attack on a metal-alkene complex, or (iii) MHAT.

MHAT represents an alkene functionalization mechanism common to TM-catalyzed Markovnikov transformations[12,13,41] such as the Mukaiyama hydration that could be responsible for the phosphine-catalyzed Markovnikov hydroamination reaction (Fig. 3A). As potential support for this proposal, the Studer group has reported a phosphine-promoted alkene hydrogenation via MHAT from a phosphoranyl radical **INT-1**[41]. Adventitious water, or the azole, could serve as the source of a hydrogen atom in the hydroamination reaction, followed by C–N bond formation via oxidative radical polar crossover of the resulting secondary carbon radical **INT-2**. However, no hydrogenation byproducts are observed (e.g. hexane), even with increased thiol loading; furthermore, the minor byproducts detected (**2A** and **2B**) imply the intermediacy of a primary radical, which is incompatible with this mechanism. We also ruled out the MHAT mechanism on the basis that it would require reduction of the P^V byproduct[42] – a stoichiometric reagent in the Studer hydrogenation – and oxidation of the unactivated secondary radical **INT-2**, neither of which is feasible given the photocatalyst potentials[43].

We thus turned to nucleophilic alkene functionalization mechanisms (i) and (ii), which would both involve the intermediacy of a phosphine radical cation (**INT-3A**) (Fig. 3B, top). To

evaluate these proposals, we sought evidence that the phosphine was the primary quencher of the excited state photocatalyst. Stern-Volmer studies indicate that both PPh_3 and P(*p*-OMePh)$_3$ quench the excited-state photocatalyst (see supplementary materials, Fig, S2). Therefore, phosphine radical cation (**INT-3A)** is likely a productive intermediate in Markovnikov-selective hydroamination. P(*p*-OMePh)$_3$, a more electron-rich phosphine, is required when employing azole substrates that can undergo competitive oxidation by the excited-state photocatalyst (see supplementary materials, Fig. S4). Alkenes are known to add to phosphine radical cations to form distonic radical cations (**INT-4**) with the positive charge primarily localized on phosphorus and the spin primarily localized on carbon[34,44]. Accordingly, radical functionalization of this intermediate at carbon is known in a limited but growing number of cases[29,45,46], most commonly via HAT or intramolecular radical cyclization onto the aryl substituents on phosphorous (Fig. 3B, top)[44,47,48]. Our observation that increased thiol loading reduced product yield and increased phosphonium salt (**B1**) formation in the optimization studies (*vide supra*, extended data Table 1, entries 4–6) is consistent with the intermediacy of a distonic radical cation (**INT-4A**), which could undergo competitive HAT with TRIP-SH. Notably, monitoring a standard reaction by ^{31}P NMR showed that **B1** is not consumed under the reaction conditions, and hexane, a formally hydrogenated byproduct that could result from C–P cleavage of the phosphonium, is not observed. Subjecting **B2**, a phosphonium salt analog of **B1**, to the catalytic conditions in the absence of added phosphine led to no desired hydroamination product (Fig. 3B, bottom), indicating that neither direct P–C scission of **B2**, nor reduction of **B2** to its corresponding phosphoranyl radical followed by α-scission, are occurring under the reaction conditions. Indeed, reduction of the phosphonium to the phosphoranyl radical ($E_{1/2}$ = –2.41 V vs. SCE) by $Ir^{(II)}$ ($E_{1/2}$ = –1.43 V vs. SCE) or $Ir^{(III)*}$ ($E_{1/2}$ = –0.92 V vs. SCE) is thermodynamically unlikely[43]. As a result, we concluded that phosphonium

salts **B1**, and **INT-5,** which could arise from oxidative radical polar crossover and nucleophilic trapping from **INT-4A**, are not productive intermediates in C–N bond formation.

Hence, we propose that C–N bond formation proceeds from **INT-4** to generate phosphoranyl radical **INT-6** – implicating a nucleophilic amination of the distonic phosphine radical cation **INT-4** – an elementary step that is not known, to the best of our knowledge. Analogous to the pathways (i) and (ii) in which transition metals catalyze nucleophilic alkene functionalization, two pathways can be considered for nucleophilic amination of the distonic radical cation **INT-4**: (ia) nucleophilic attack of azole at phosphorus to afford a P^V intermediate, followed by (ib) radical migratory insertion to the carbon-centered radical via **TS-1**, or (ii) direct nucleophilic addition–intramolecular SET between the azole and distonic radical cation (**TS-2**) (Fig. 3C). Pathway (ii) can be considered as the microscopic reverse of a spin-center shift (SPS) process[33], wherein addition of a polar nucleophile, the azole, pushes the odd electron into an adjacent anti-bonding orbital. While the acceptor orbitals in most SPS processes are π* in character, this proposed mechanism suggests that similar chemistry is also possible with P–C antibonding orbitals. Subsequent α-scission from phosphoranyl radical **INT-6** to give terminal radical **INT-7** is kinetically facile and thermodynamically favorable ($\Delta G^{\ddagger}$ = +6.3 kcal/mol, ΔG = –14.7 kcal/mol, see supplementary materials, Fig. S44). Notably, the generation of byproducts **2A** and **2B** is consistent with the intermediacy of **INT-7** and indicates that this activation mode could enable the development of a suite of regioselective alkene difunctionalization reactions.

We sought to experimentally evaluate the feasibility of the nucleophilic amination step based on physical organic reactivity principles. In transition metal-catalyzed nucleophilic amination of alkenes, the carbon that undergoes C–N bond formation develops a partial positive charge following coordination to the metal center. Under the hypothesis that a similar process

could be occurring in our system via either of the nucleophilic amination pathways (i) or (ii), we investigated a potential linear free energy relationship (LFER) through competition studies using substituted styrene partners and N–H azole **1** (Fig. 3D). A LFER was observed with σ_p values, but not radical σ values (see supplementary materials, Figs. S33 and S34) with a ρ value of –1.0. Similar ρ values have been observed for transition metal-catalyzed nucleophilic functionalization reactions of styrenes in relation to alkene coordination[49–52]. In our system, the alkene addition step to the phosphine radical cation, which would also display a negative LFER, has been suggested to be fast and reversible[44,46]. Therefore, the negative ρ value is more likely to be a readout of the rate-determining C–N bond formation step, consistent with buildup of positive charge at carbon in the bond-forming transition state (*vida infra*). Consistent with this step being rate-determining, an inverse secondary kinetic isotope effect ($k_H/k_D = 0.95$) was observed via competition experiment using styrene-α-d_1 (see supplementary materials, section 9).

We hypothesized that if a nucleophilic amination is responsible for C–N bond formation, an alkene bearing a β-silicon group could interrupt C–N bond formation via an intramolecular elimination and electron transfer according to the β-silyl effect, providing further evidence for the polar nature of the C–N bond formation (Fig. 3E). In this case, β-elimination of trimethylsilyl cation would be expected to afford phosphoranyl radical **INT-8** from **INT-4B**, which upon α-scission and HAT, would generate propene in situ. If silyl radical were to eliminate instead, a phosphonium byproduct would be detected which could not undergo subsequent P–C cleavage. Under the standard reaction conditions, reaction of N–H azole **1** with allyltrimethylsilane (**43**) afforded *N-iso*-propylated product **44** in 47% yield with observation of propene, consistent with the proposed nucleophilic functionalization of the distonic radical cation.

As a final test of the proposed C–N bond formation, we sought to evaluate radical cyclization substrates **45** and **46** (Fig. 3F). We hypothesized that if C–N bond formation is assisted via P – either in the stepwise (i) or concerted mechanism (ii) – radical cyclization substrates that displace the C-centered radical from the phosphonium prior to C–N bond formation would not afford aminated products. Specifically, with diethyl diallylmalonate (**45**), the proposed distonic radical cation would be expected to undergo fast intramolecular 5-*exo*-trig cyclization[53,54] to **INT-4C** prior to intermolecular C–N bond formation. Since the carbon radical in **INT-4C** is located further from the cationic phosphorus, we expected that C–N bond formation would not take place. Consistent with this hypothesis, we observe no *N*-alkylated products, but phosphine is fully consumed according to ^{31}P NMR, likely to the phosphonium salt after competitive HAT. Conversely, with a radical cyclization substrate that would undergo slow radical cyclization from the distonic radical cation, but fast cyclization from the resulting primary radical post α-scission, we would expect formation of *N*-alkylated product. Indeed, with 1,5-hexadiene (**46**), we observed 83% yield of **48**, which we attribute to formation via a favorable 5-*exo*-trig cyclization ($k = \sim 2 \times 10^5$ s^{-1})[53] from the terminal radical that results from α-scission of **46a**.

We then turned to DFT to provide additional support for the feasibility of the nucleophilic amination step and further distinguish between a stepwise (ia) nucleophilic addition followed by (ib) migratory insertion or a (ii) direct nucleophilic addition – intramolecular single electron transfer (SET). Using P(*p*-OMePh)$_3$ as catalyst, methylene cyclopentane as alkene and 3-phenylpyrazole as azole, we found a stable pentavalent phosphorane **INT-9** that proceeds through **TS-1** to phosphoranyl radical **INT-6A** (Fig. 4A, solid pathway), supporting the first pathway for nucleophilic amination. Comparison of the P–N and P–C bond lengths in **INT-9** and **TS-1** suggests an asynchronous migratory insertion, which led us to identify a transition state **TS-2** that would

arise from pathway (ii), which has a higher activation energy but is still kinetically feasible ($\Delta\Delta G^{\ddagger}$ = +16.5 kcal/mol, $\Delta\Delta G$ = –13.8 kcal/mol) (Fig. 4A, dotted pathway). An NBO charge and spin analysis on **INT-9** and **TS-1**, and **INT-4D** and **TS-2**, respectively (Fig. 4B), reveals a similar loss of electron density at carbon and an increase in radical spin density at phosphorus, consistent with our linear free energy relationship (Fig. 3D) suggesting that either nucleophilic amination pathway could be operative.

Given the structural variety of azoles that are compatible in the reaction, we wondered if the likelihood of either pathway could be distinguished by substrate identity, with direct nucleophilic addition–intramolecular SET between the azole and distonic radical cation preferred for bulkier azoles. To interrogate this possibility further, we calculated the potential energy surface of this nucleophilic amination pathway for azabenzimidazole **14**. For the Markovnikov-selective conditions, we did not find a stable pentacoordinate **INT-9**-type intermediate for this substrate combination representative of pathway (i); however, transition states corresponding to direct nucleophilic addition–intramolecular SET were identified, representative of pathway (ii). To validate the feasibility of this pathway, we questioned whether our calculations could rationalize the complete *N1*-site selectivity observed experimentally. Indeed, under the proposed C–N bond formation manifold, the computed activation barriers for *N1* vs *N3* alkylation reveal a $\Delta\Delta G\ddagger$ of 4.9 kcal/mol favoring *N1* alkylation (Fig. 4C). Distortion-Interaction analysis of the two transition states suggests there to be greater interaction between the azole and distonic radical cation for N1 nucleophilic attack, as well as reduced distortion from the ground state for the distonic radical cation (see supplementary materials, Table S53 for computational details), consistent with steric control on the transition state imparted by the differences in azole structure and subsequent approach to the distonic radical cation.

Last, we sought to understand the influence of phosphine identity on reaction regiochemical outcome (Fig. 4D). Our previous report for anti-Markovnikov selectivity indicated NCR addition to the alkene to be both rate and selectivity-determining. Under the Markovnikov conditions, nucleophilic amination is proposed to be rate-determining. The selectivity switch between the anti-Markovnikov selective PCy_3 and Markovnikov-selective P(*p*-OMePh)$_3$ catalysts likely arises from differences in relative kinetic barriers of the two competing rate-determining steps. To probe this hypothesis, we calculated the potential energy surface of the Markovnikov nucleophilic amination pathway for PCy_3 as the phosphine catalyst and compared it to that arising with P(*p*-OMePh)$_3$ when methylene cyclopentane was employed as the alkene partner. When P(*p*-OMePh)$_3$ is catalyst, alkene addition is followed by a fast and irreversible nucleophilic amination via migratory insertion transition state **TS-1** ($\Delta G^{\ddagger}$ = +15.0 kcal/mol, ΔG = –13.1 kcal/mol) from a transient pentavalent phosphorus intermediate **INT-9**, leading to the Markovnikov product. In comparison, following azole addition and α-scission, NCR **INT-10** addition to the alkene via **TS-3** was calculated to be kinetically disfavored by +2.2 kcal/mol ($\Delta G^{\ddagger}$ = +17.2 kcal/mol, ΔG = –15.7 kcal/mol). However, with PCy_3, Markovnikov C–N bond formation was calculated to occur directly through nucleophilic addition – intramolecular SET of distonic radical cation **INT-4D′** via **TS-2′** ($\Delta G^{\ddagger}$ = +21.1 kcal/mol, ΔG = –6.5 kcal/mol), and was computed to be kinetically and thermodynamically less favorable than NCR addition by +3.9 kcal/mol, ultimately leading to anti-Markovnikov selectivity. Distortion-Interaction analysis of **TS-1** and **TS-2′** suggests similar distortion and interaction effects for both transition states from the ground state distonic radical cation and azole (see supplementary materials, Table S55); hence, likely entropic penalties for **INT-4D′** to **TS-2′** contribute most significantly to the disparity in kinetic barriers. Furthermore, delocalization of the P–C phosphoranyl radical **INT-6A** into the aromatic π-system of P(*p*-

OMePh)$_3$ stabilizes the intermediate and to a greater extent, **TS-1**, in contrast to what is possible with PCy$_3$[55].

Based on these combined experimental and computational observations, we propose the following catalytic cycle for the Markovnikov hydroamination (Fig. 3G). Trivalent phosphine PAr$_3$ is oxidized through a photocatalytic reductive quenching cycle to **INT-3**. Alkene addition into **INT-3** generates distonic radical cation **INT-4**. **INT-4** undergoes the proposed nucleophilic addition–intramolecular SET or (ia) nucleophilic addition–(ib) migratory insertion C–N bond formation to **INT-6**. The P–C(sp^3) bond of **INT-6** undergoes preferential homolysis to form **INT-7** and regenerate the trivalent phosphine. HAT with the thiol catalyst furnishes the *N*-alkylated product and simultaneously closes the photocatalytic cycle after electron transfer and proton transfer.

In conclusion, we leverage the reactivity of distonic phosphine radical cations with nucleophilic partners to develop a regioselective intermolecular hydroamination of a range of unactivated, terminal alkenes with numerous, distinct N–H azoles. The catalytic protocol complements existing radical-based anti-Markovnikov strategies and Markovnikov-selective, transition metal-catalyzed methods that often face substrate limitations. Our mechanistic understanding of the phosphine-catalyzed nucleophilic alkene functionalization step suggests avenues for extending the reactivity to the development of other valuable synthetic methods.

References

1. Power, P. P. Main-group elements as transition metals. *Nature* **463**, 171–177 (2010).

2. Lipshultz, J. M., Li, G. & Radosevich, A. T. Main Group Redox Catalysis of Organopnictogens: Vertical Periodic Trends and Emerging Opportunities in Group 15. *J. Am. Chem. Soc.* **143**, 1699–1721 (2021).

3. Melen, R. L. Frontiers in molecular p-block chemistry: From structure to reactivity. *Science* **363**, 479–484 (2019).

4. Müller, T. E., Hultzsch, K. C., Yus, M., Foubelo, F. & Tada, M. Hydroamination: Direct Addition of Amines to Alkenes and Alkynes. *Chem. Rev.* **108**, 3795–3892 (2008).

5. Trowbridge, A., Walton, S. M. & Gaunt, M. J. New Strategies for the Transition-Metal Catalyzed Synthesis of Aliphatic Amines. *Chem. Rev.* **120**, 2613–2692 (2020).

6. Coombs, J. R. & Morken, J. P. Catalytic Enantioselective Functionalization of Unactivated Terminal Alkenes. *Angew. Chem. Int. Ed.* **55**, 2636–2649 (2016).

7. Huang, L., Arndt, M., Gooßen, K., Heydt, H. & Gooßen, L. J. Late Transition Metal-Catalyzed Hydroamination and Hydroamidation. *Chem. Rev.* **115**, 2596–2697 (2015).

8. Ma, S. & Hartwig, J. F. Progression of Hydroamination Catalyzed by Late Transition-Metal Complexes from Activated to Unactivated Alkenes. *Acc. Chem. Res.* **56**, 1565–1577 (2023).

9. Müller, T. E. & Beller, M. Metal-Initiated Amination of Alkenes and Alkynes †. *Chem. Rev.* **98**, 675–704 (1998).

10. Shevick, S. L. *et al.* Catalytic hydrogen atom transfer to alkenes: a roadmap for metal hydrides and radicals. *Chem. Sci.* **11**, 12401–12422 (2020).

11. Sevov, C. S., Zhou, J. (Steve) & Hartwig, J. F. Iridium-Catalyzed, Intermolecular Hydroamination of Unactivated Alkenes with Indoles. *J. Am. Chem. Soc.* **136**, 3200–3207 (2014).

12. Yahata, K., Kaneko, Y. & Akai, S. Cobalt-Catalyzed Intermolecular Markovnikov Hydroamination of Nonactivated Olefins: N 2-Selective Alkylation of Benzotriazole. *Org. Lett.* **22**, 598–603 (2020).

13. Miao, H. *et al.* Photoredox and Cobalt-Catalyzed Markovnikov-Selective Radical Hydroamination of Unactivated Alkenes with Anilines. *Org. Lett.* **27**, 3296–3301 (2025).

14. Mol, J. C. Industrial applications of olefin metathesis. *J. Mol. Catal. A: Chem.* **213**, 39–45 (2004).

15. Ertl, P. & Schuhmann, T. A Systematic Cheminformatics Analysis of Functional Groups Occurring in Natural Products. *J. Nat. Prod.* **82**, 1258–1263 (2019).

16. Marshall, C. M., Federice, J. G., Bell, C. N., Cox, P. B. & Njardarson, J. T. An Update on the Nitrogen Heterocycle Compositions and Properties of U.S. FDA-Approved Pharmaceuticals (2013–2023). *J. Med. Chem.* **67**, 11622–11655 (2024).

17. Larsen, M. A. & Hartwig, J. F. Iridium-Catalyzed C–H Borylation of Heteroarenes: Scope, Regioselectivity, Application to Late-Stage Functionalization, and Mechanism. *J. Am. Chem. Soc.* **136**, 4287–4299 (2014).

18. Liu, Y.-J. *et al.* Overcoming the limitations of directed C–H functionalizations of heterocycles. *Nature* **515**, 389–393 (2014).

19. Das, R., Daniliuc, C. G. & Hahn, F. E. Oxidative Addition of 2-Halogenoazoles—Direct Synthesis of Palladium(II) Complexes Bearing Protic NH,NH-Functionalized NHC Ligands. *Angew. Chem. Int. Ed.* **53**, 1163–1166 (2014).

20. Bogdos, M. K., Müller, P. & Morandi, B. Structural Evidence for Aromatic Heterocycle N–O Bond Activation via Oxidative Addition. *Organometallics* **42**, 211–217 (2023).

21. Escorihuela, J., Lledós, A. & Ujaque, G. Anti-Markovnikov Intermolecular Hydroamination of Alkenes and Alkynes: A Mechanistic View. *Chem. Rev.* **123**, 9139–9203 (2023).

22. Moon, H. W. & Cornella, J. Bismuth Redox Catalysis: An Emerging Main-Group Platform for Organic Synthesis. *ACS Catal.* **12**, 1382–1393 (2022).

23. Légaré, M.-A., Pranckevicius, C. & Braunschweig, H. Metallomimetic Chemistry of Boron. *Chem. Rev.* **119**, 8231–8261 (2019).

24. Hilton, M. C. *et al.* Heterobiaryl synthesis by contractive C–C coupling via P(V) intermediates. *Science* **362**, 799–804 (2018).

25. Zhang, X. *et al.* Phosphorus-mediated sp2–sp3 couplings for C–H fluoroalkylation of azines. *Nature* **594**, 217–222 (2021).

26. Lim, S. & Radosevich, A. T. Round-Trip Oxidative Addition, Ligand Metathesis, and Reductive Elimination in a PIII/PV Synthetic Cycle. *J. Am. Chem. Soc.* **142**, 16188–16193 (2020).

27. Fujimoto, H., Kodama, T., Yamanaka, M. & Tobisu, M. Phosphine-Catalyzed Intermolecular Acylfluorination of Alkynes via a P(V) Intermediate. *J. Am. Chem. Soc.* **142**, 17323–17328 (2020).

28. Bonfante, S., Lorber, C., Lynam, J. M., Simonneau, A. & Slattery, J. M. Metallomimetic C–F Activation Catalysis by Simple Phosphines. *J. Am. Chem. Soc.* **146**, 2005–2014 (2024).

29. Li, J., Zhang, Y., Zhu, S. & Chu, L. Photocatalyzed Dicyanation of Alkenes Enabled by Phosphorus Radical Cation Addition. *Chem. A Eur. J.* e202501154 (2025) doi:10.1002/chem.202501154.

30. Kang, B. *et al.* Visible Light Promotes PIII/PV-Catalyzed Reductive N-Arylation of Nitroarenes at Room Temperature. *ACS Catal.* 12477–12483 (2025) doi:10.1021/acscatal.5c04341.

31. Smidt, Dr. J. *et al.* Katalytische Umsetzungen von Olefinen an Platinmetall-Verbindungen Das Consortium-Verfahren zur Herstellung von Acetaldehyd. *Angew. Chemie.* **72**, 176–182 (1959).

32. Kawatsura, M. & Hartwig, J. F. Palladium-Catalyzed Intermolecular Hydroamination of Vinylarenes Using Arylamines. *J. Am. Chem. Soc.* **122**, 9546–9547 (2000).

33. Zhang, F.-L., Li, B., Houk, K. N. & Wang, Y.-F. Application of the Spin-Center Shift in Organic Synthesis. *JACS Au* **2**, 1032–1042 (2022).

34. Chinn, A. J., Sedillo, K. & Doyle, A. G. Phosphine/Photoredox Catalyzed Anti-Markovnikov Hydroamination of Olefins with Primary Sulfonamides via α-Scission from Phosphoranyl Radicals. *J. Am. Chem. Soc.* **143**, 18331–18338 (2021).

35. Sedillo, K., Fan, F., Knowles, R. R. & Doyle, A. G. Cooperative Phosphine-Photoredox Catalysis Enables N–H Activation of Azoles for Intermolecular Olefin Hydroamination. *J. Am. Chem. Soc.* **146**, 20349–20356 (2024).

36. Sevov, C. S., Zhou, J. (Steve) & Hartwig, J. F. Iridium-Catalyzed Intermolecular Hydroamination of Unactivated Aliphatic Alkenes with Amides and Sulfonamides. *J. Am. Chem. Soc.* **134**, 11960–11963 (2012).

37. Zhang, Z., Lee, S. D. & Widenhoefer, R. A. Intermolecular Hydroamination of Ethylene and 1-Alkenes with Cyclic Ureas Catalyzed by Achiral and Chiral Gold(I) Complexes. *J. Am. Chem. Soc.* **131**, 5372–5373 (2009).

38. Inoue, M., Sumii, Y. & Shibata, N. Contribution of Organofluorine Compounds to Pharmaceuticals. *ACS Omega* **5**, 10633–10640 (2020).

39. Pennington, L. D. & Moustakas, D. T. The Necessary Nitrogen Atom: A Versatile High-Impact Design Element for Multiparameter Optimization. *J. Med. Chem.* **60**, 3552–3579 (2017).

40. Hassam, M., Taher, A., Arnott, G. E., Green, I. R. & Otterlo, W. A. L. van. Isomerization of Allylbenzenes. *Chem. Rev.* **115**, 5462–5569 (2015).

41. Zhang, J., Mück-Lichtenfeld, C. & Studer, A. Photocatalytic phosphine-mediated water activation for radical hydrogenation. *Nature* **619**, 506–513 (2023).

42. Santhanam, K. S. V. & Bard, A. J. Electrochemistry of organophosphorus compounds. II. Electroreduction of triphenylphosphine and triphenylphosphine oxide. *J. Am. Chem. Soc.* **90**, 1118–1122 (1968).

43. Teegardin, K., Day, J. I., Chan, J. & Weaver, J. Advances in Photocatalysis: A Microreview of Visible Light Mediated Ruthenium and Iridium Catalyzed Organic Transformations. *Org. Process Res. Dev.* **20**, 1156–1163 (2016).

44. Liu, K. *et al.* Photon-driven radical hydro-phosphoniumylation of unactivated olefins. *Chem Catal.* **5**, (2024).

45. Ando, T., Yokogawa, D., Ohmatsu, K. & Ooi, T. Deoxygenative [3 + 2] Annulation of α,β-Unsaturated Carbonyl Compounds and Electron-Rich Olefins via Photocatalytic Umpolung of Triarylphosphine. *J. Am. Chem. Soc.* (2025) doi:10.1021/jacs.5c06114.

46. Qiu, J., Zhang, X., Zheng, H. & Zhu, G. Photocatalytic Phosphine-Mediated Deoxygenative [3 + 2] Cycloaddition of α,β-Unsaturated Carbonyls and Alkenes. *J. Am. Chem. Soc.* **147**, 19004–19012 (2025).

47. Masuda, Y., Tsuda, H. & Murakami, M. Photoinduced Dearomatizing Three-Component Coupling of Arylphosphines, Alkenes, and Water. *Angew. Chem. Int. Ed.* **60**, 3551–3555 (2021).

48. Masuda, Y., Uno, M. & Murakami, M. Photoinduced Reaction of Triarylphosphines with Alkenes Forming Fused Tricyclic Phosphonium Salts. *Org. Lett.* **23**, 8445–8449 (2021).

49. Michel, B. W., Steffens, L. D. & Sigman, M. S. On the Mechanism of the Palladium-Catalyzed tert-Butylhydroperoxide-Mediated Wacker-Type Oxidation of Alkenes Using Quinoline-2-Oxazoline Ligands. *J. Am. Chem. Soc.* **133**, 8317–8325 (2011).

50. Burger, B. J., Santarsiero, B. D., Trimmer, M. S. & Bercaw, J. E. Kinetics and Mechanism of the Insertion of Olefins into Niobium- and Tantalum-Hydride Bonds: A Study of the Competition between Steric and Electronic Effects. *J. Am. Chem. Soc.* (1988) doi:10.1021/ja00218a023.

51. Hanley, P. S. & Hartwig, J. F. Intermolecular Migratory Insertion of Unactivated Olefins into Palladium–Nitrogen Bonds. Steric and Electronic Effects on the Rate of Migratory Insertion. *J. Am. Chem. Soc.* **133**, 15661–15673 (2011).

52. Rix, F. C., Brookhart, M. & White, P. S. Electronic Effects on the β-Alkyl Migratory Insertion Reaction of para-Substituted Styrene Methyl Palladium Complexes. *J. Am. Chem. Soc.* **118**, 2436–2448 (1996).

53. Beckwith, A. L. J. & Schiesser, C. H. Regio- and stereo-selectivity of alkenyl radical ring closure: A theoretical study. *Tetrahedron* **41**, 3925–3941 (1985).

54. Griller, D. & Ingold, K. U. Free Radical Clocks. *Acc. Chem. Res.* 317–323 (1980) doi:10.1021/ar50153a004.

55. Evans, M. G. & Polanyi, M. Inertia and Driving Force of Chemical Reactions. *Trans. Faraday Soc.* 11–24 (1938) doi:10.1039/tf9383400011.

Figure legends:

Fig. 1 | Introduction. a, Transition-metal catalyzed nucleophilic amination with terminal alkenes and limitations. **b,** Mimicking transition metal catalysis with phosphorous. **c,** Unexplored activation modes in phosphorus catalysis. **d,** Phosphine-catalyzed Markovnikov-selective hydroamination with terminal alkenes.

Fig. 2 | Azole and Alkene Scope. Reactions were performed on a 0.5 mmol scale using 1.0 equiv of azole and 3.0 equiv of alkene, PPh_3 or P(*p*-OMePh)$_3$ (20 mol%), [Ir(dF(Me)ppy)$_2$dtbbpy]PF_6 (2 mol%), and TRIP-SH (10 mol%) irradiating with 450 nm LEDs for 18 h. Isolated yield reported as an average of two runs. [a]PPh_3 was used as the phosphine catalyst. [b]P(*p*-OMePh)$_3$ was used as the phosphine catalyst. [c]Reaction run at 0.05 M with 2 x 427 nm Kessil lamps. [d]Isolated yield from reaction performed on 5 mmol scale. [e]Reaction run with P(*p*-OMePh)$_3$ (20 mol%), analytical ^{1}H NMR yield determined by comparison to an internal standard of 1,3,5-trimethoxybenzene, reaction set up on the bench, sparging with N_2 for 5 minutes followed by addition of alkene, instead of in a glovebox. [f]Analytical ^{1}H NMR yield determined by comparison to an internal standard of 1,3,5-trimethoxybenzene, reaction set up under Schlenk technique instead of in a glovebox. [g]Reaction run with 2.0 equiv. of alkene. [h]Reaction run with P(*p*-OMePh)$_3$ (20 mol%), 1.2 equiv. of alkene, and TRIP–SH (20 mol%). [i]Analytical ^{1}H NMR yield determined by comparison to an internal standard of 1,3,5-trimethoxybenzene.

Fig. 3 | Mechanistic Studies. a, Considering a metal-catalyzed hydrogen atom transfer mechanism; side products isolated and characterized. **b,** Ruling out alternative reactivity pathways from distonic radical cation; reaction performed on 0.1 mmol scale with [Ir(dF(Me)ppy)$_2$dtbbpy]PF_6 (2 mol%), TRIP-SH (10 mol%), and $PhCF_3$ (0.1 M), irradiating with 450 nm LEDs for 18 h., absence of products observed by ^{1}H NMR of reaction mixture. **c,** Proposed C–N bond formation involving nucleophilic amination via (ia) nucleophilic addition – (ib) migratory insertion or nucleophilic addition – intramolecular SET. **d,** Hammett relationship from competition studies performed on 0.1 mmol scale with 1.0 equiv. 3-phenylpyrazole and 1.5 equiv. each of styrene and *para*-substituted styrene; relative yields as a proxy for log(*k*X/*k*H) were determined by ^{1}H NMR spectroscopic analysis. **e,** Isolated yield on 0.5 mmol scale; propene observed by ^{1}H NMR for 0.1 mmol scale reaction in toluene-*d*8 in a J-Young tube. **f,** Radical cyclization experiments; top: absence of *N*-alkylated product observed by ^{1}H NMR of reaction mixture; bottom: isolated yield on 0.5 mmol scale with PPh_3 (20 mol%) as phosphine catalyst. **g,** Proposed mechanism for Markovnikov selectivity.

Fig. 4 | DFT Computational Studies. a, Reaction coordinate or proposed C–N bond formation with 3-phenylpyrazole, methylene cyclopentane, and P(*p*-OMePh)$_3$ phosphine catalyst; free energies were calculated at the (U)M06-2X/def2-TZVP/SMD(Toluene)//(U)M06-2X/def2-SVP level of theory and reported in kcal/mol. Hydrogen atoms omitted for clarity, bond lengths reported

in Angstroms, and reaction coordinate not drawn to scale. **b,** CYLview structures (left, in panels) and spin density difference plots (right, in panels); NBO charge and spin density values obtained from calculations performed at the same level of theory and basis set. **c,** *N1*-site selectivity of substrate **14** supported by kinetic barrier differences in the nucleophilic addition–intramolecular SET step; calculations performed at the (U)M06-2X/def2-TZVP/SMD(Toluene)//(U)M06-2X/def2-SVP level of theory; energy values reported in kcal/mol, reaction coordinate not drawn to scale. **d,** General scheme and computational investigation of phosphine-dependent regioselectivity outcomes with 3-phenylpyrazole and methylene cyclopentane substrates; NBO spin density difference plots of TS-1 and TS-2′ shown; reference ground states set to distinct intermediates for comparison of RDS, relative kinetic barriers and thermodynamic free energies for P(*p*-OMePh)$_3$ (black) vs. PCy$_3$ (grey) were calculated at the (U)M06-2X/def2-TZVP/SMD(Toluene)//(U)M06-2X/def2-SVP level of theory, energy values reported in kcal/mol.

Methods: Experimental and computational procedures for this study are available in the supplementary materials.

Data availability: Experimental procedures, characterization data, and DFT calculations supporting the findings of this study are available in the supplementary materials. X-ray crystallographic data are available free of charge from the Cambridge Crystallographic Data Centre, under reference number 2476334.

Additional references: N/A

Acknowledgments: Financial support was provided by National Institutes of Health (NIGMS R35 GM126986). A.J.M. acknowledges support from NSF Graduate Research Fellowship Program (DGE-2034835). We acknowledge support from NSF shared instrumentation grant CHE-1048804 and NIH Office of Research Infrastructure Programs shared instrumentation grant S10OD028644. Computational and storage services associated with the Hoffman2 Shared Cluster were provided by UCLA Institute for Digital Research and Education's Research Technology Group. We thank T. Judah Raab for assistance with X-Ray structure determination. We also thank Dr. Emily R. Wearing, Prof. Alexander Q. Cusumano, and Prof. Robert R. Knowles for helpful discussions and directions.

Author contributions: F.F. designed, performed, and analyzed the experiments and computations. K.F.S. discovered the initial result. A.J.M. wrote the submission script template for DFT computations. A.G.D. designed and supervised the overall research project. F.F. and A.G.D. wrote the manuscript with inputs from all authors.

Competing interests: The authors declare no competing interests.

Additional information: The online version contains supplementary material available at…. Correspondence and requests for materials should be addressed to A.G.D. Peer review information… Reprints and permissions information is available at www.nature.com/reprints.

Extended data legends:

Extended Data Table 1 | Optimization Studies.

Unless specified otherwise, reactions were performed on a 0.1 mmol scale reacting 1.0 equiv of 3-phenylpyrazole with 3.0 equiv of 1-hexene, $[Ir(dF(Me)ppy)_2dtbbpy]PF_6$ (2 mol%), and TRIP-SH (10 mol%) irradiating with 450 nm LEDs for 18 h. Yields were determined by ^1H NMR spectroscopic analysis against 1,3,5-trimethoxybenzene as an internal standard.

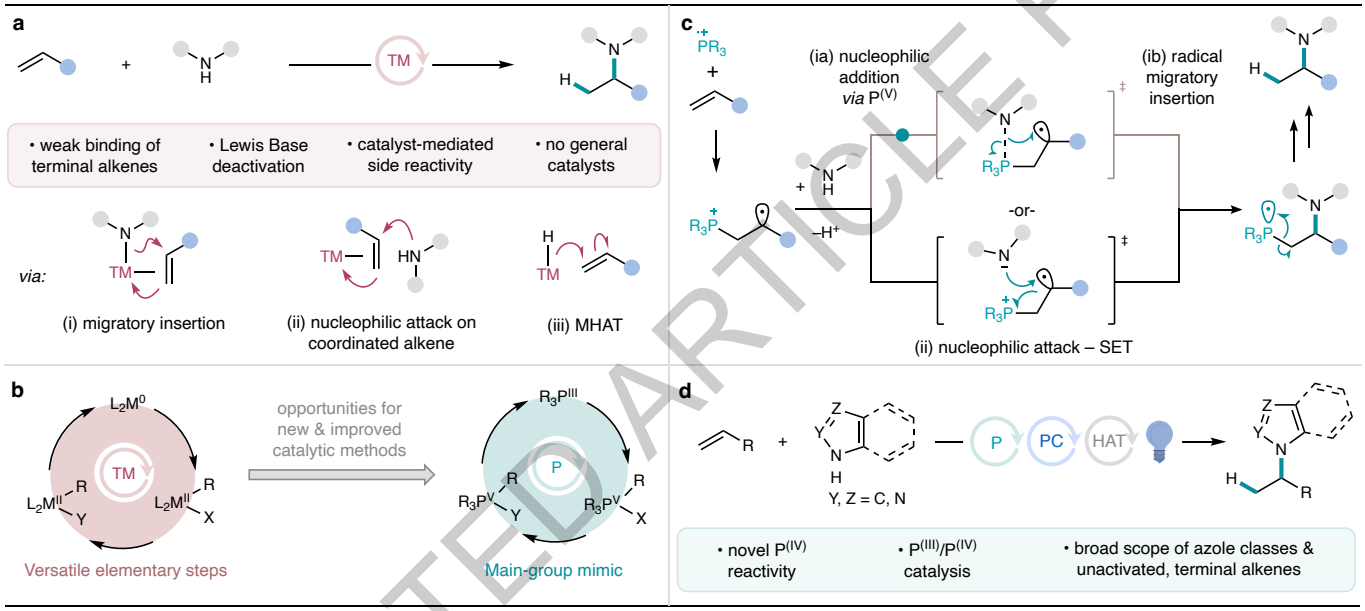

Pyrazoles[a]

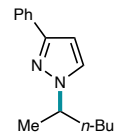

2
85% yield[d]
76% yield[b,e]

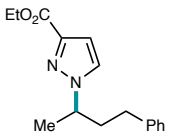

3
78% yield

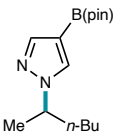

4
26% yield

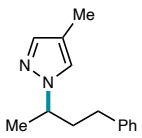

5
57% yield
from fomepizole

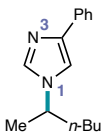

6
75% yield
68% yield[f]

Imidazoles[b]

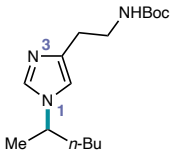

7
64% yield
from Boc-histamine

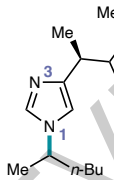

8
29% yield, *d.r. 1:1*
from dexmedetomidine

Indazoles[a,c]

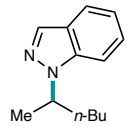

9
63% yield

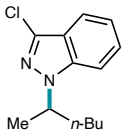

10
80% yield

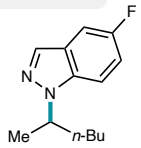

11
65% yield

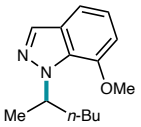

12
50% yield

Benzimidazoles[b]

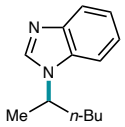

13
55% yield

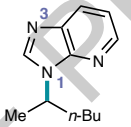

14
41% yield

Triazole[a]

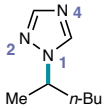

15
68% yield

Azaindoles[b]

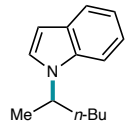

16
42% yield

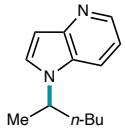

17
57% yield

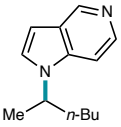

18
48% yield

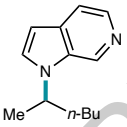

19
61% yield

Carbazole[b]

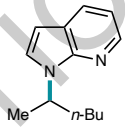

20
34% yield

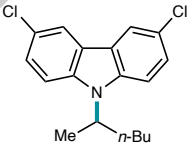

21
43% yield

Oxindole[b]

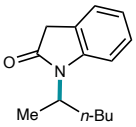

22
44% yield

Ureas[b]

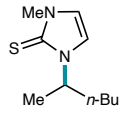

23
52% yield
from methimazole

Carbamate[b]

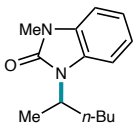

24
75% yield

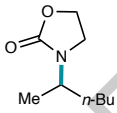

25
49% yield

1 equiv. each additive in reaction of **2**

>50% yield with additive

recovered additive:
>50%
<50%
<20%

Functional group compatibility

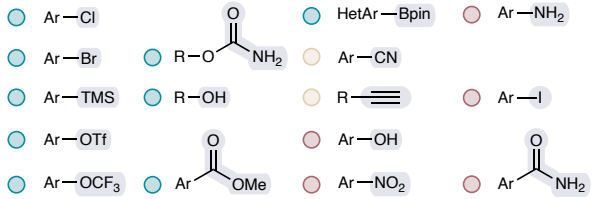

Unactivated alkenes[a]

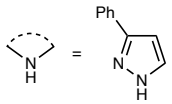

1

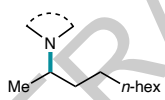

26
70% yield

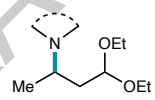

27
75% yield

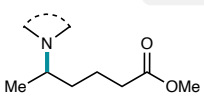

28
77% yield

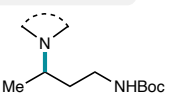

29
79% yield

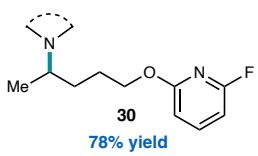

30
78% yield

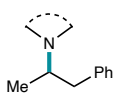

31
59% yield

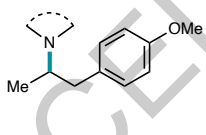

32
69% yield
from estragole

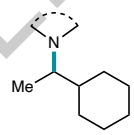

33
90% yield

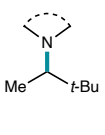

34
89% yield

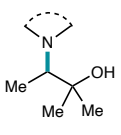

35
90% yield

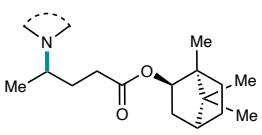

36
89% yield, *d.r 1:1*
from (–)-borneol

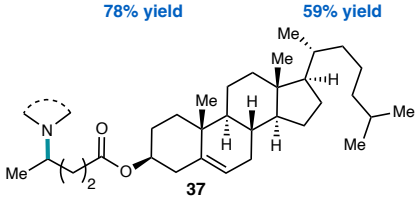

37
78% yield[g], *d.r. 1:1*
from cholesterol

1,1-disubstituted

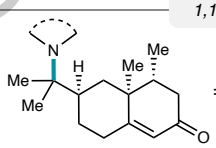

38
26% yield
from (+)-nootkatone

39
20% yield

Activated[h]

40
65% yield

41

Internal

with P(*p*-OMePh)$_3$:
14% yield[i]
r.r. 1 to 1.6 C1:C2

with PCy_3:
38% yield[i]
r.r. 1 to 6.4 C1:C2

42

with P(*p*-OMePh)$_3$:
13% yield
exclusive C1

with PCy_3:
2% yield[i]
exclusive C2

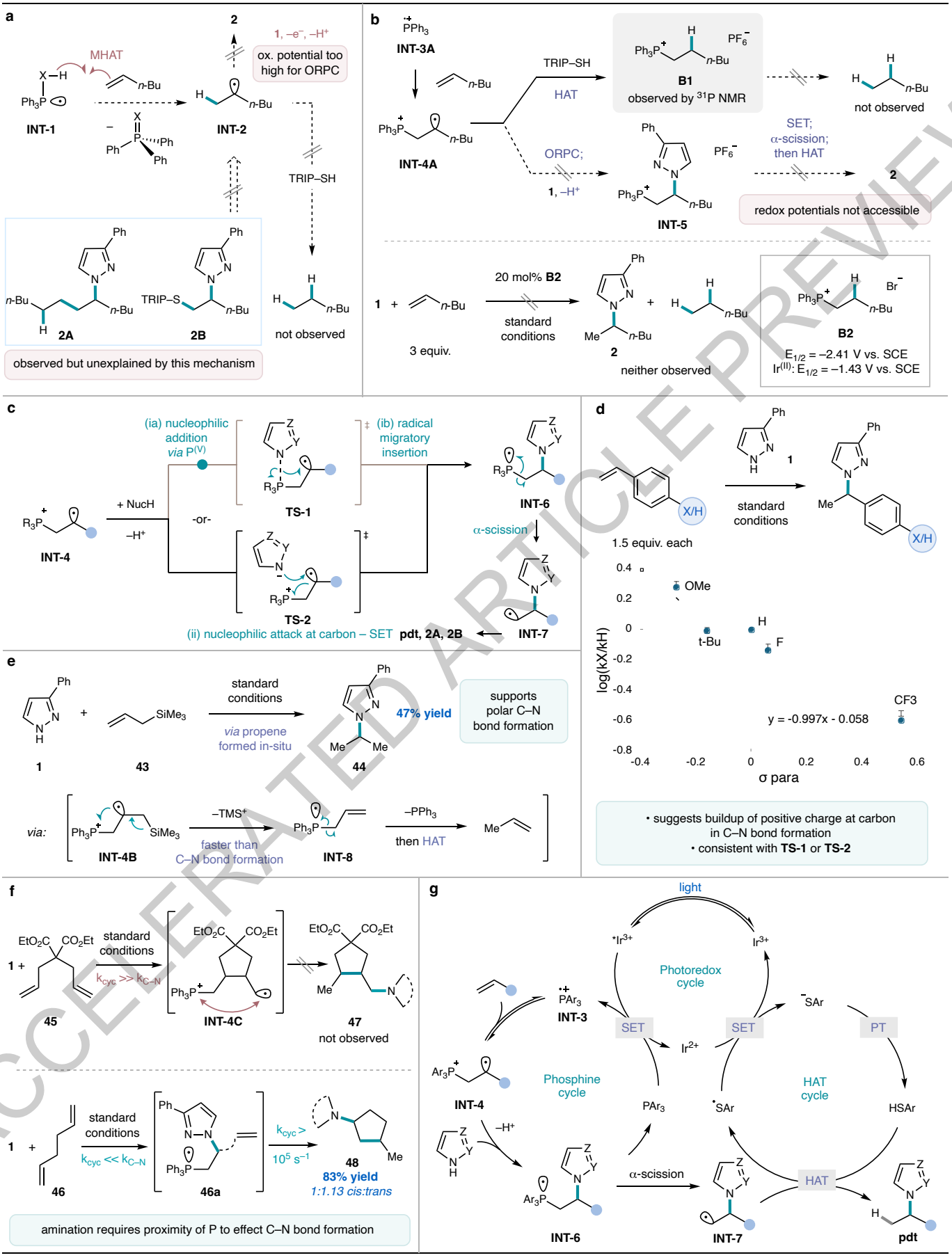

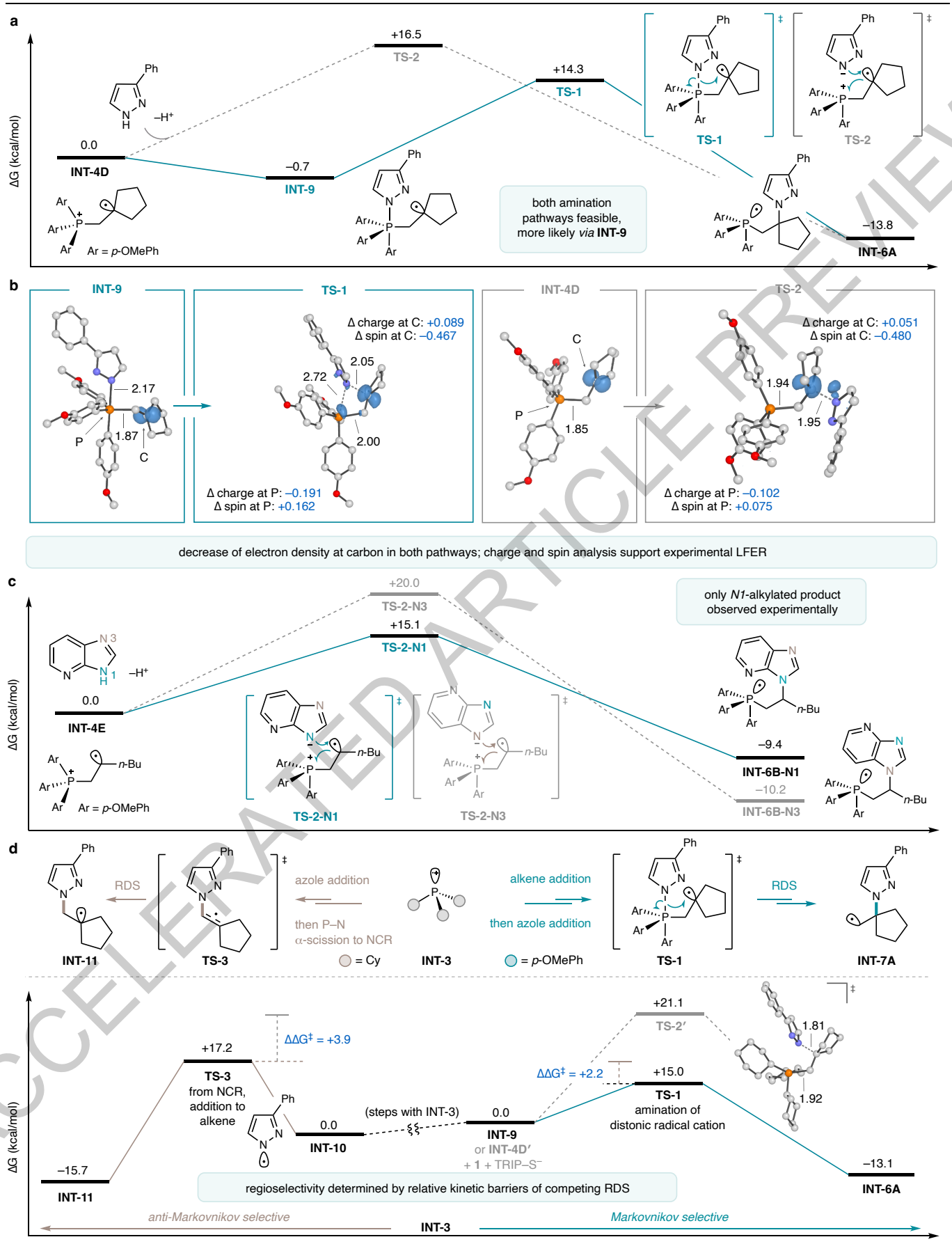

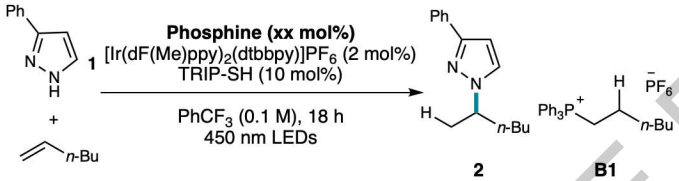

Entry	Phosphine	Phosphine loading (mol%)	Yield of **2** (%)
1	$P(p\text{-}OMePh)_3$	20	**93**
2	PPh_3	20	**89**
3	PPh_3	10	**9**

Entry	Phosphine (20 mol%)	Thiol loading (mol%)	Yield of **B1** (% of P species)	Yield of **2** (%)
4	PPh_3	20	24	**83**
5	PPh_3	50	33	**44**
6	PPh_3	100	69	**6**

Entry	Modification from entry 2	Yield of **2** (%)
7	10 mol% $Pd(OAc)_2$, $Cu(OAc)_2$, $NiBr_2$, or $Fe(acac)_3$	**0**
8	No phosphine	**0**
9	No photocatalyst	**0**
10	No TRIP-SH	**7**
11	No light	**0**
12	1 equiv. 1-hexene	**64**
13	1 equiv. 1-hexene, 48 h	**86**

Extended Data Table 1